Effect of Titanium Dioxide Nanoparticles on the Redox Regulatory Network of Cells

A Dissertation Presented to the Academic Faculty

By

Dipesh Khanal

In Partial Fulfillment of the Requirements for the Degree

Master of Science in Chemistry

Georgia Institute of Technology

May 2015

Effect of Titanium Dioxide Nanoparticles on the Redox Regulatory Network of Cells

Approved by:

Dr. Christine Payne, Advisor

School of Chemistry and Biochemistry

Georgia Institute of Technology

Dr. Melissa Kemp

Wallace H. Coulter Department of Biomedical Engineering

Georgia Institute of Technology

Dr. Amit Reddi

School of Chemistry and Biochemistry

Georgia Institute of Technology

Date Approved: 04/23/2015

TABLE OF CONTENTS

ACKNOWLEDGMENTS

I would like to thank Dr. Christine Payne for mentoring me throughout this research project and serving as the chair of my thesis committee. I would also like to thank rest of the committee members, Dr. Melissa Kemp and Dr. Amit Reddi, for their suggestions and guidance in writing this thesis. Working in the Payne Lab with some awesome people has been a great experience and I would like to acknowledge all the current and previous lab members for their suggestions and comments. I would also like to thank the HERCULES Exposome Research Center for providing financial support for this project.

LIST OF TABLES

LIST OF FIGURES

SUMMARY

The extensive industrial and commercial use of titanium dioxide nanoparticles (TiO_2 NPs) in paints, cosmetics, and as food coloring additives is associated with high levels of TiO_2 NPs released into the environment and subsequent human exposure. Previous studies have linked TiO_2 NPs exposure to reactive oxygen species (ROS) production in cells; however, the exact mechanism between oxidative stress and cellular toxicity is unknown. We hypothesize that cellular binding and/or internalization of TiO_2 NPs leads to a shift in transcriptional expression of oxidative stress related genes. As a first step, we investigated the size distribution of TiO_2 NPs in different biologically relevant media. Our results show that TiO_2 NPs agglomerate into large particles, and are comparatively smaller in human serum (200-700 nm) than in water (800-1500 nm). The formation of a protein corona, verified by gel electrophoresis, contributes to decreased aggregation in human serum. TiO_2 NPs exposure to the cells, followed by reverse transcriptase polymerase chain reaction (qPCR) analysis of oxidative stress related genes (in collaboration with Prof. Melissa Kemp, BME) has led to the identification of the genes with altered expression. Specifically, peroxiredoxin 1 and peroxiredoxin 5 showed up regulation, whereas peroxiredoxin 3 and peroxiredoxin 4 showed down regulation. This approach of probing the redox response of cells in terms of collective gene expression, rather than focusing on a single pathway, will provide a whole cell mechanistic model of nanoparticle-induced oxidative stress.

CHAPTER 1

INTRODUCTION

Titanium dioxide nanoparticles (TiO_2 NPs), also referred to as titania, are a class of metal oxide nanoparticles. Besides their use in industrial products such as paints and lacquers, TiO_2 NPs are used extensively in daily consumer products such as sunscreens, toothpastes, and cosmetic items (1, 2). Another main application of TiO_2 NPs is in wastewater treatment plans, where they are utilized for their photocatalytic properties to get rid of organic pollutants (3). TiO_2 is a white pigment and because of its brightness and high refractive index, it is the choice of pigment used in the industries accounting for about 70% of total pigment production in the world (4). TiO_2 is one of the most widely used nanoscale material to date, and even though bulk TiO_2 contributes to most of the annual production, TiO_2 NPs are beginning to take over the market. TiO_2 NPs have a higher refractive index and additional surface area in comparison to its bulk counterpart, which makes it suitable in lot of applications that require high opacity, corrosion resistance and photocatalytic activity (5). It is estimated that by 2024, all of the bulk TiO_2 will be replaced by TiO_2 NPs (6). The annual production of TiO_2 is estimated to be around 4 million metric tons. This high production of TiO_2 NPs is associated with a release into the environment (6).

Human exposures to TiO_2 NPs occur during both manufacturing and use. There are three possible routes of exposure to TiO_2 NPs: ingestion, inhalation, and dermal (7). Gastrointestinal absorption is an important exposure route for TiO_2 NPs since lot of food materials are known to contain these nanoparticles as either additives or coloring agents. Biodistribution experiment in mice showed that TiO_2 NPs mainly retained in the liver, spleen, kidneys, and lung tissues after uptake by gastrointestinal tract (7). Dermal absorption is another possible route of exposure to TiO_2 NPs. Rodent studies so far have shown that TiO_2 NPs penetrated into vacant hair follicles; however, they do not penetrate into live tissue even when the conditions are mimicked for small injuries in the skin (8). Pulmonary absorption through inhalation is another possible route of TiO_2 NPs exposure, especially in industrial workers. Even though

studies lack human data for inhalation studies, it has been shown that TiO_2 NPs can translocate from the lung into the circulatory system and from nasal cavity into the sensory nerves in rodents (9).

Oxygen has an important role in various biological processes, including generation of energy in the form of adenosine triphosphate (ATP) production in the mitochondria. It has been estimated that almost 5% of total inhaled oxygen is converted into several damaging ROS species like superoxide, hydroxyl and hydrogen peroxide (10). This conversion process in the body is normal part of our physiology and is essential for various cellular activity. Mostly immune response through phagocytosis, detoxification of xenobiotics, cell growth, and induction of mitogenic responses are some of the cellular processes which are beneficial outcomes of low concentration ROS. In addition to that, low concentration of ROS also play an important role in activation of cytokines, growth factor signaling, activation of nuclear transcription factors and second messenger activities (10).

Despite these advantages, when ROS are present in higher concentrations, they disrupt the redox homeostasis of cells. There are several enzymes such as superoxide dismutase (SOD), glutathione peroxidases (GPx) and various other antioxidants which help maintain this redox balance by being oxidized themselves. When a biological system has a reduced capacity to counteract overproduction or invasion of reactive oxygen species and other radicals, then this state is known as oxidative stress. During this stage lipids, proteins, DNA or the entire cell can be damaged. Lipids present in subcellular organelles are highly sensitive to reactive oxygen species. When ROS react with lipids, a chain reaction of lipid peroxidation is initiated which results in disruption of fluidity and permeability (10). One particular study found that TiO_2 NPs delivered to the abdominal cavity caused oxidative stress and injury in mice brains (9), and the mechanism was attributed to lipid peroxidation. Similarly, proteins are also highly susceptible to ROS which interfere with the enzymatic activity and function of structural proteins, by modification of amino acid side chains. Normal cell function could be disrupted when proteins involved in signal transduction pathway such as receptors or ion channel proteins interact with

nanoparticles leading to activation or deactivation of certain pathways (11). A study showed that TiO_2 NPs inhibit enzyme activity and induce conformational changes in arylamine N-acetyltransferase, a xenobiotic metabolizing enzyme involved in detoxification of carcinogens (12). Protein hydroperoxides are generated by oxidation of proteins caused by ROS, which gradually accumulate over time and contribute to damage associated with ageing and other diseases (10). DNA damage is also another issue related with high concentration of ROS. Especially, hydroxyl (•OH) radical is known to affect both purine and pyrimidine bases in the DNA and produce purine/pyrimidine oxidative products. ROS attack also causes activation of poly (ADP-ribose) synthetase enzyme which can lead to fragmentation of DNA (8). Oxidative stress is associated with premature aging and other conditions, including cancer, Alzheimer's, autism, cardiovascular diseases, pulmonary disorders, autoimmune diseases, and gastrointestinal disorders (10).

Nanoparticles may come into contact to a human body either directly from using associated products, or indirectly following their release into the environment. This is especially relevant to TiO_2 NPs because of their huge annual production (6). Previous work has shown that oxidative stress is a common cellular response to nanoparticles, which ultimately leads to nanotoxicity (13). TiO_2 NPs are known to produce reactive oxygen species (ROS) in response to UV activation in biological systems. Production of excess ROS is a major contributor to nanotoxicity as it creates an oxidative stress in cells (14).

Previous studies have linked cellular health degradation with exposure to TiO_2 NPs. A decrease in cell viability, mitochondrial activity and ATP levels was observed in A549 lung cells (15). This decrease in cellular health markers is associated with the production of ROS. Another study by Long et. al. found out that mouse microglia respond to TiO_2 NPs with cellular and morphological expressions of free radical formation (16). It has been well established that TiO_2 NPs display a very high production of ROS under UV irradiation (13, 14, and 15).

Our method in investigating the toxicity of TiO_2 NPs is unique compared to studies done in the past due to the following two distinct features: First, we have mimicked environmental conditions by using unsonicated particles in the form of agglomerates for all cellular studies. Secondly, an investigation of genetic expression change is evaluated for 84 oxidative stress related genes, to evaluate an entire cellular system rather than a single pathway.

Most TiO_2 NPs toxicity studies have used particles those of primary sizes ranging from 5nm to 200 nm, which are agitated using ultrasonic frequencies (sonication) before exposing to the biological component of the experiment. However, no such mechanism exist naturally that prevents aggregation, and thus it is crucial to study them in the same form they exist in the environment. Nanoparticle size plays an important role in determining the internalization behavior into the cells. Previous studies have shown that unsonicated TiO_2 NPs remain as aggregate ranging from 165nm to 375 nm in cell culture media, regardless of their primary individual particle size, which was 20nm (15). Therefore, for our studies, it is expected that TiO_2 NPs will be present in the form of aggregates and this will be investigated using dynamic light scattering (DLS).

After initial exposure of TiO_2 NPs, they can distribute into organs and tissues in the body through systemic circulation. Even though studies have shown that only a fraction of inhaled TiO_2 NPs get into the circulatory system, routine exposure is a potential issue (10). Ultimately, they come in contact with the blood serum composed of plasma-proteins, coagulation factors, platelets and red/white blood cells. Human blood serum is a protein rich environment, where albumin is the most abundant protein (55%) alongside immunoglobulins (38%), fibrinogens (7%) and other proteins in trace amounts (17). It is well established that a protein layer forms on nanoparticle surface upon exposure to a protein rich environment, for example, in human serum (18, 19). The protein corona also dictates the internalization process by binding to specific receptors on cell membrane. Previous study in our lab have shown that a major component of the protein corona on the surface of polystyrene nanoparticle is albumin (19). We

expect a similar trend for TiO_2 NPs and hypothesize that TiO_2 NPs will have a protein corona in which albumin would be a major component. This hypothesis is tested using gel electrophoresis to verify the presence of corona, and mass spectrometry to identify composition.

Previous studies on the effect of TiO_2 NPs have focused on the toxicity of nanoparticles, however, lacked the exact biochemical mechanism. Instead of focusing on a single pathway, our approach focuses on change in gene expression across a wide range of oxidative stress related genes. This experimental approach has been used by the Kemp Lab to investigate non-targeted alterations in the redox network due to lentiviral infection and shRNA silencing of glutaredoxin, thioredoxin and G6PD (20). We have investigated 84 different oxidative stress related genes and quantified the changes in gene expression using reverse transcriptase – polymerase chain reaction (RT-PCR). Cell viability assays (MTT) and membrane permeabilization assays (LDH) were carried out as measures of cell health. Western blot was used to verify the level of protein expression for some of the genes we have identified through RT-PCR.

This initial investigation into the redox network of cells has a broad impact for environmental health and safety, as it focuses on the effect of TiO_2 NPs present in the environment on cellular oxidative stress. Development of such models to predict changes to oxidative stress is not only limited to TiO_2 NPs but the experimental methods developed in the course of this research is applicable to any nanoparticle of interest. With this knowledge about the effect of nanoparticles and any other chemical compound found in the environment which we live in, we can make better decisions about minimizing the adverse effects.

CHAPTER 2

TiO_2 NP CHARACTERIZATION

2.1 Transmission electron microscopy (TEM)

Titanium (IV) oxide (TiO_2, #718467) nanoparticles were purchased from Sigma-Aldrich. Transmission electron microscope (TEM, JEOL 100CX II), located at the Center for Nanostructure Characterization at Georgia Institute of Technology, was used to characterize the size of titanium dioxide nanoparticles (TiO_2 NPs). The analysis was performed at 100kV and 200kx magnification. TiO_2 NPs, as shown in the images (figure 1), were observed in the form of agglomerates and were non-spherical. As seen in figure 2, the agglomerates also had empty groove like spaces within themselves, and these spaces were larger for some agglomerates compared to others. This shows that TiO_2 NPs agglomerates do not have a fixed shape and qualitatively it can be inferred that they are different in terms of their size as well. However, the individual particles seem to be similar in shape and size.

As a calibration method, the pixel length of scale bar from the raw image was measured by using line tool, a command in the ImageJ program. Three different measurements were taken for the scale bar from three images, using the largest end to end distance for asymmetrical agglomerates. The average pixel length that corresponded to the 25 nm length scale bar was 58 pixels. A scale factor of 1 nm for 2.32 pixels was determined. This scale factor was used to calculate the size of the agglomerates and individual particles within.

The diameter distribution of TiO_2 agglomerates ranged from 100 nm to 500 nm, with an average of 290 nm. This average diameter was calculated from 10 different agglomerates (table 1). The primary particle size listed in the manufacturer's label (Sigma Aldrich) was 21 nm. Individual particle diameter was found to be in the range of 10 nm to 35 nm with an average of 24 nm, which was computed from 20 random individual particles from the TEM images.

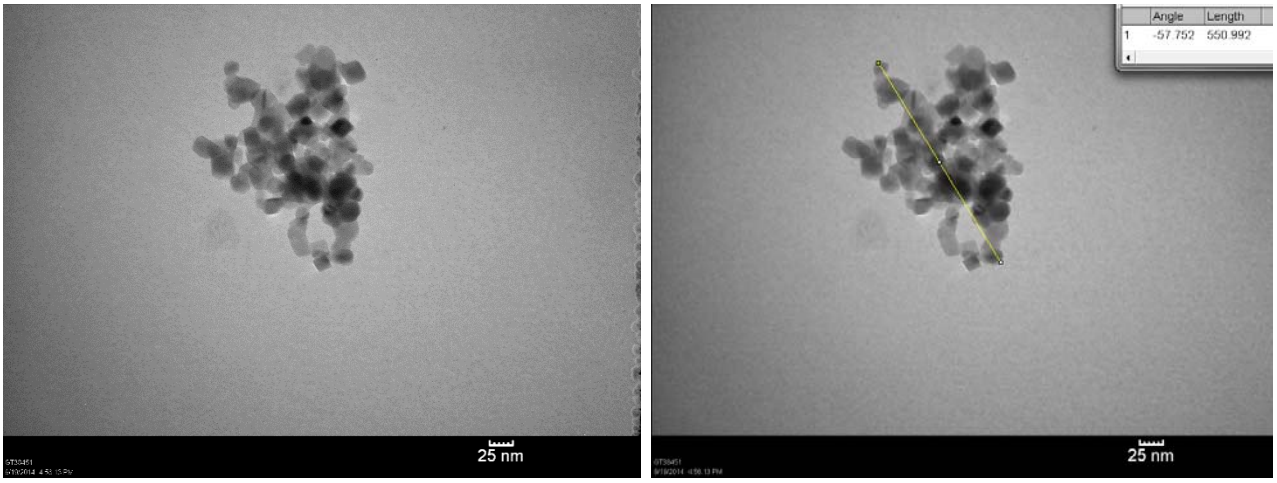

Fig. 1: Analysis of a TEM image TiO_2 NP agglomerate: A raw image is shown on the left. To find the end to end length of the agglomerate, a line is drawn (yellow) using ImageJ (NIH) and the distance is calculated in pixel units, which is later converted to nm based on scale factor (1 nm = 2.32 pixels).

Table 1: TiO_2 NP agglomerate diameter in pixels and nm across 10 samples

Agglomerate	Diameter (pixels)	Diameter (nm)
1	293	126
2	688	296
3	977	421
4	610	262
5	521	224
6	479	206
7	1159	499
8	794	342
9	354	152
10	843	363

Table 2: TiO_2 NP individual particle diameter in pixels and nm across 20 samples

Individual particle	Diameter (pixels)	Diameter (nm)		Individual particle	Diameter (pixels)	Diameter (nm)
1	49.5	21.3		11	72.1	31.0
2	65.5	28.2		12	43.8	18.9
3	46.0	19.8		13	43.8	18.9
4	60.9	26.2		14	28.4	12.2
5	56.1	24.1		15	52.1	22.4
6	65.5	28.2		16	68.4	29.4
7	53.2	22.9		17	43.8	18.9
8	57.3	24.7		18	60.0	25.8
9	51.6	22.2		19	43.2	18.6
10	79.6	34.3		20	82.2	35.4

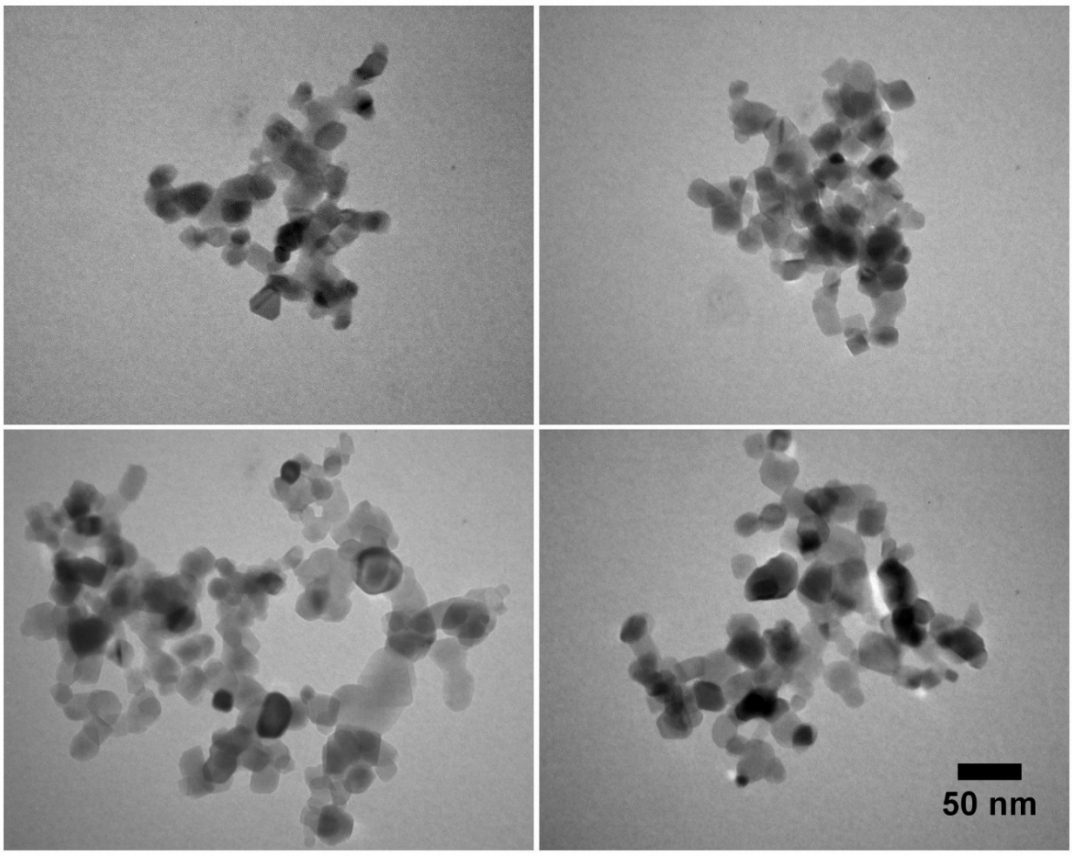

Fig. 2: Transmission electron microscopy images show that TiO_2 NPs are agglomerates rather than individual particles.

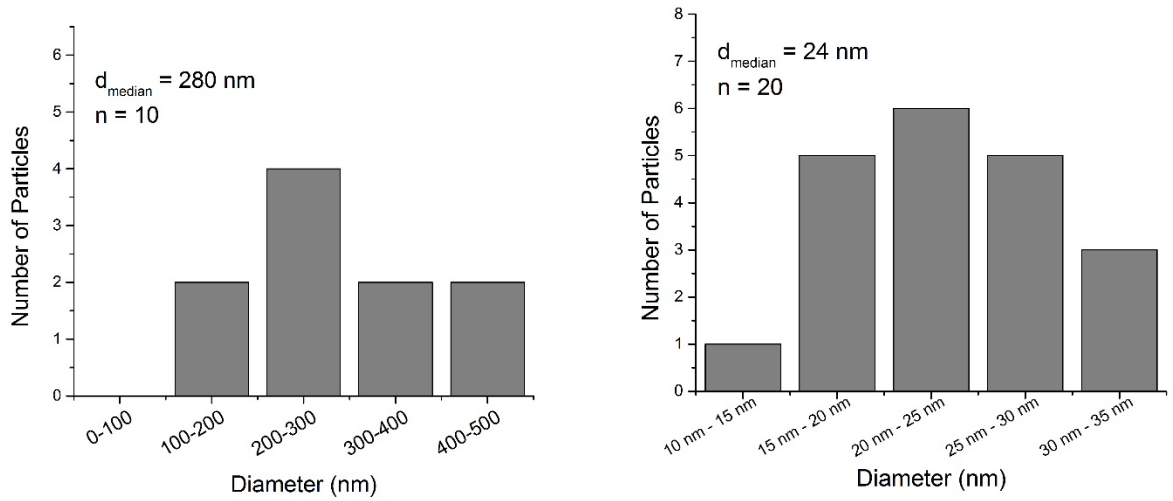

Fig. 3: Size distribution of TiO_2 nanoparticles as seen from TEM images: median diameter is 280 nm, which is determined from 10 different agglomerates (left). Individual particles have a median diameter of 24 nm, from 20 random particles.

2.2 Dynamic Light Scattering (DLS)

Dynamic Light Scattering (DLS) is an important tool for characterizing the size of nanoparticles in solution. The principle behind this analysis is based on the movement of particles in suspension, also known as Brownian motion. This type of motion of particles causes laser light to be scattered at different intensities. Analysis of the modulation of the scattered light intensity as a function of time provides the hydrodynamic diameter and polydispersity of the nanoparticles. Larger particles will diffuse more slowly than smaller particles and the DLS measures the time dependence of the scattered light to generate a correlation function which then is used to determine particle size using Stoke-Einstein equation below:

$$D_z = \frac{k_B T}{3\pi\eta D_{(t,avg)}}$$

D_z = hydrodynamic diameter,

k_B = Boltzmann's constant (1.38×10^{-23} J/K)

T = temperature,

η = viscosity of medium

$D_{t,avg}$ = diffusion coefficient.

Nanoparticle size has an important role in the effect it induces on the cells. Previous studies have shown that small particles have a greater surface area and therefore more sites of reaction compared to larger particles which have less surface area that is exposed. A study has shown that unsonicated TiO_2 NPs remain as aggregate ranging from 165nm to 375 nm in cell culture media, regardless of their primary individual particle size of 20nm. It is essential to characterize the size of the nanoparticles in our studies as the size determines the internalization and binding of unsonicated TiO_2 NPs with the cells.

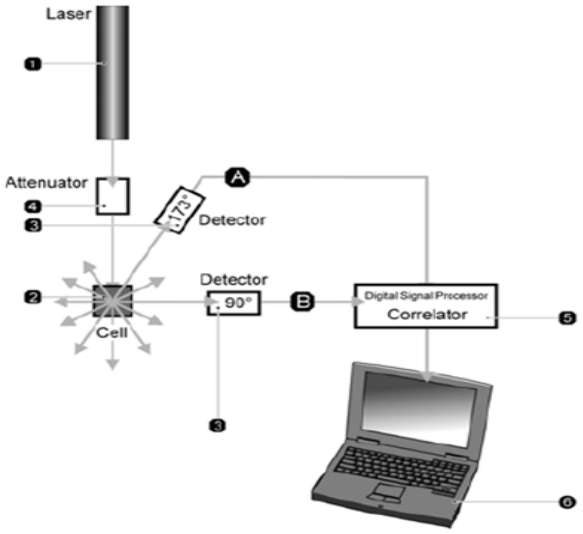

Fig 4: Schematic representation of a DLS instrument (Image obtained from Malvern Instruments. http://www.malvern.com/)

Materials:

Titanium (IV) oxide (TiO_2, #718467) was purchased from Sigma-Aldrich. Human Serum (BP1600 100) was purchased from Fisher Scientific. Dynamic Light Scattering (DLS, Malvern Instruments, Nano-ZS) was used to measure the hydrodynamic diameter. 30 μg/mL TiO_2 nanoparticles were incubated in 10% human serum (v/v in PBS) for 10 minutes. All measurements were performed in triplicates for three samples.

Effect of Sonication:

First, the effect of sonication on the size distribution of TiO_2 nanoparticles was investigated. This initial characterization was crucial because most of the studies done in the past have focused on particles that

have been sonicated. However, under environmental conditions and especially nanoparticles escaping the waste water treatment plans are not subject to sonication.

A concentration range of 3 µg/mL to 300 µg/mL TiO_2 was used in this study and it was observed that under sonication for 30 minutes the particle size was much smaller compared to no sonication. The average hydrodynamic diameter was well above 850 nm for all three concentrations for the non-sonicated particles. As expected, the sonicated particles were much smaller, with average diameter around 300 nm. At the same time, the polydispersity index (PDI) of sonicated sample was also low (0.2 – 0.4), while non-sonicated samples had very high polydispersity index (> 0.5). Polydispersity index is used to determine how disperse the nanoparticles are in the sample. A high PDI indicates the sample has a very broad distribution of size amongst the particles, whereas, a smaller PDI means the diameter of the particles are very close with each other. In other words, a high PDI represents a heterogeneous mixture of TiO_2 NPs and a low PDI represents a homogenous mixture.

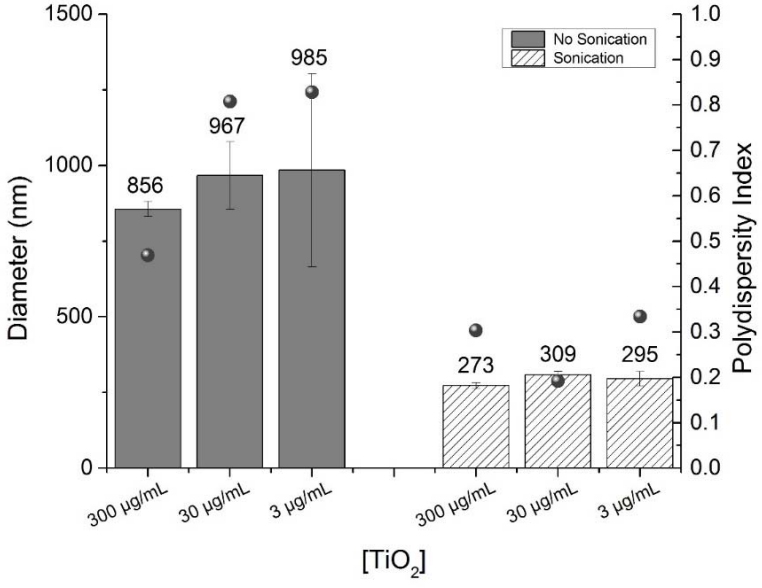

Fig 5: Comparison of average hydrodynamic diameter and polydispersity between sonicated (lines) and non-sonicated (solid grey) TiO_2 nanoparticles in water

Size distribution in biological media:

It was hypothesized that the presence of a charged species such as protein, or a buffer environment such as phosphate buffered saline (PBS) may alter the aggregation state and hydrodynamic diameter of TiO_2 nanoparticles. DLS was performed on 30 µg/mL of TiO_2 NPs in water and 10% (v/v) human serum supplemented PBS. As expected from previous result (15), the particles were in the form of agglomerates in water with a median hydrodynamic diameter of 1.1 µm. However, in PBS-serum the median diameter was 369 nm, with agglomerates ranging from 200 nm to 800 nm.

This huge difference in diameter can be attributed to the presence of proteins present in human serum and their surface charge. It is known that nanoparticles when exposed to a protein rich environment form a coat of proteins around them known as "protein corona". The presence of negatively charged protein domains on the surface of nanoparticles now dictates how they behave in solution. Instead of forming agglomerates, the nanoparticles now have a repulsive force that prevents them from getting close to each other. This median diameter of 369 nm is also in agreement with the TEM size (avg = 290 nm).

Table 3: Summary of size distribution of TiO_2 NPs in water and human serum

Medium	**Diameter range (nm)**	**Median diameter (nm)**
Water	800 – 1500	1100
10% human serum (v/v, PBS)	200 – 800	369

The presence of peaks in the sub 100 nm region in figure 3 suggests that TiO_2 NPs may be present in sizes smaller than 50 nm. However, DLS analysis of 10% human serum alone (Figure 4) shows that these small peaks are present even without TiO_2 NPs. Most likely, these peaks are protein aggregates which are in the human serum.

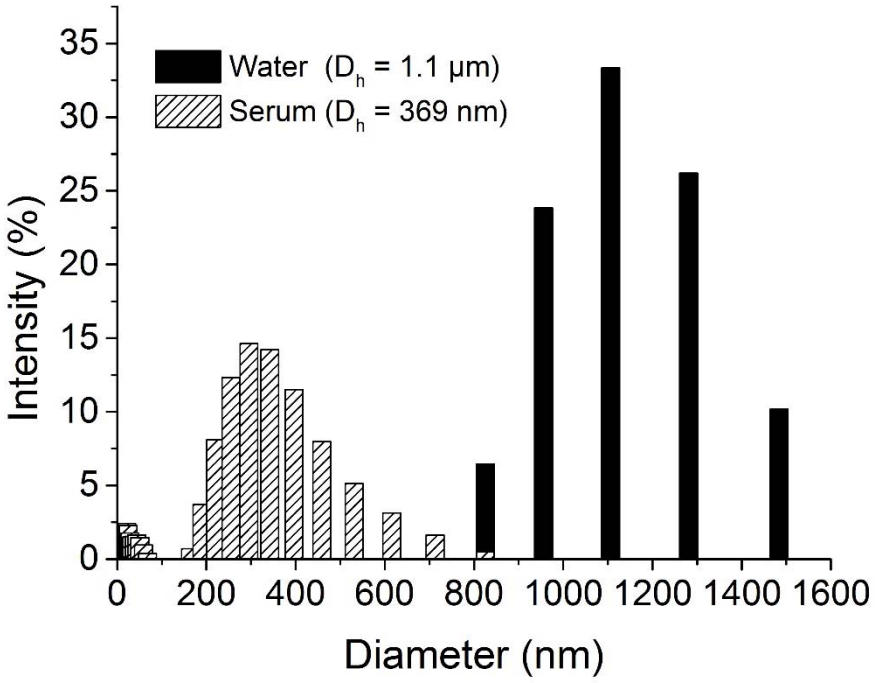

Fig 6: The hydrodynamic diameter of TiO_2 NPs in water (solid black) and 10% (v/v) human serum (solid lines)

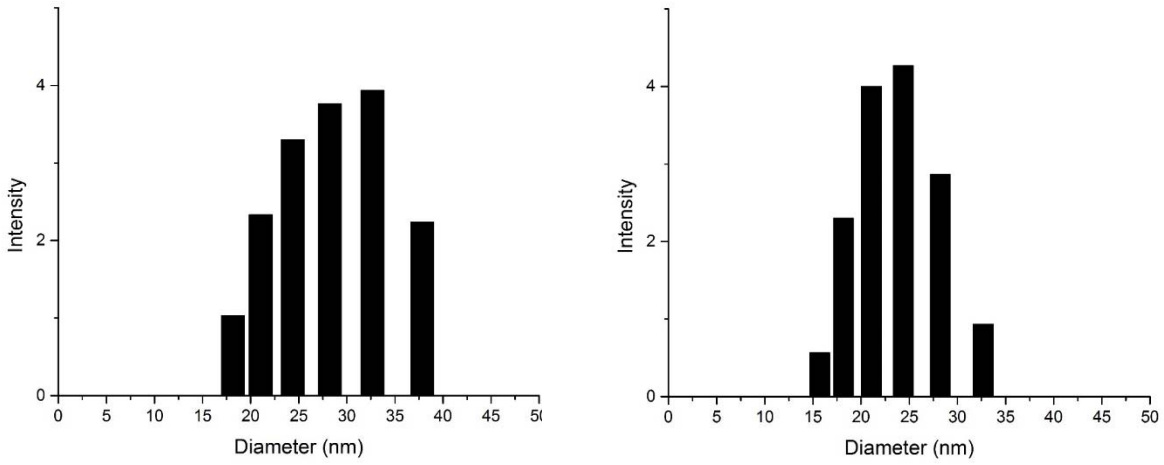

Fig 7: Size distribution in less than 100nm range for TiO_2 NPs in 10% human serum (left) and human serum alone (right).

2.3 Formation of protein corona and characterization

Nanoparticles exposed to the human body, especially in the bloodstream, encounter a number of biological components such as blood cells, clotting factors and serum proteins. Nanoparticles used for cellular experiments also get in contact with serum proteins, which are used as essential nutrients for cells. These proteins form a layer on nanoparticle known as “protein corona”. Depending on the affinity of proteins for the surface of the nanoparticle, there are two main degree of binding of the corona proteins. Hard corona proteins are bound with stronger affinity compared to soft corona proteins, which are weakly bound and can be removed using physical process such as centrifugation.

Corona proteins influence which cellular receptor is used by the protein-nanoparticle complex for entry into the cell. Previous study with polystyrene nanoparticle has shown that protein structure can be altered by adsorption on nanoparticle surface. A change in secondary structure of bovine serum albumin (BSA) adsorbed on surface of cationic nanoparticle redirects the protein-NP complex to scavenger receptor, whereas, BSA on the surface of anionic nanoparticle retains native structure and binds to albumin receptor (19). Therefore, it is important to understand the identity of the proteins that are adsorbed on the surface of the nanoparticles. For our purposes, SDS-PAGE followed by mass spectrometry was performed to verify the presence of corona and characterize its composition, following the incubation of TiO_2 nanoparticles with human serum.

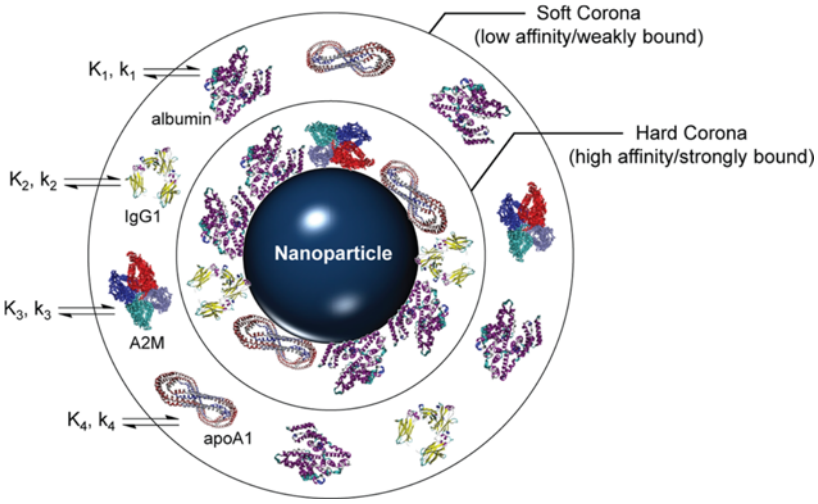

Fig 8: Schematic of protein corona formation on a nanoparticle surface. (19)

Titanium (IV) oxide (TiO_2, #718467) nanoparticles were purchased from Sigma-Aldrich. Human Serum (BP1600 100) was purchased from Fisher Scientific. Mini-PROTEAN® Precast Gel (4-20%) was purchased from Bio-Rad (#456-1094). TiO_2 nanoparticles were incubated in 10% (v/v) human serum for 30 minutes. The mixture was then centrifuged at 8000 rpm for 15 minutes (4 °C) to get rid of any unbound proteins that could be present in the supernatant. This process was followed by four centrifugation-wash steps at the same conditions. The first two washes were diluted at 1% and 10% (v/v) respectively, since they were highly concentrated with serum proteins. After each wash step the supernatant was loaded onto the wells. After four wash steps, the pellets were resuspended in water and loaded onto the well. Human serum (1%) without any nanoparticle was run for comparison.

Following the last centrifugation step, 20 µL of Laemmli SDS buffer (Boston Bioproducts, Ashland, MA) was added to the nanoparticle-protein pellet to remove protein formed on the nanoparticle surface. The sample was loaded onto a precast polyacrylamide gel in addition to a 5-225 kDa molecular weight marker (Lonza ProSieve Unstained Protein Marker, #50547, VWR, Rockland, ME). Gel electrophoresis was performed at 130 V for an hour. This was followed by staining with Simply Blue Safe Stain for an hour and destaining in water overnight.

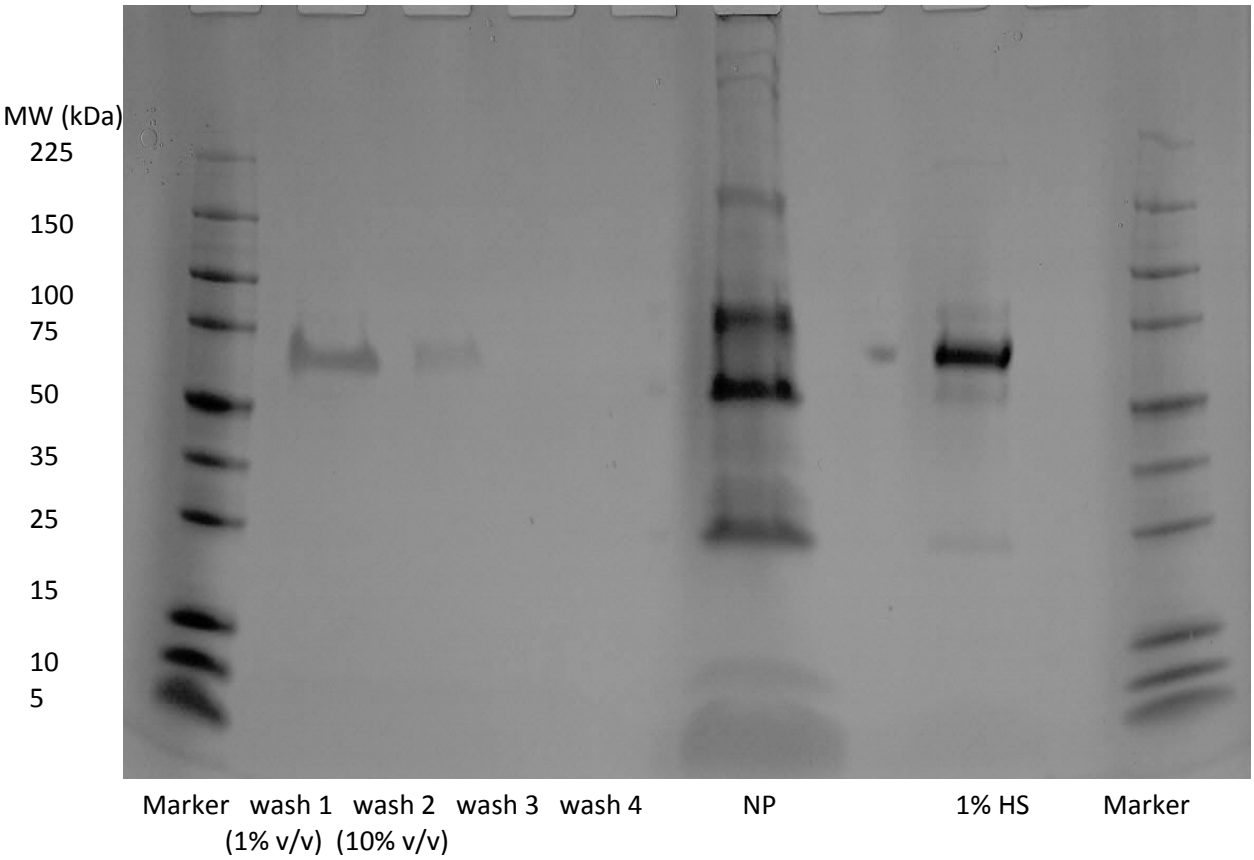

Fig 9: Formation of a protein corona on TiO_2 nanoparticles confirmed with SDS-PAGE. 1% human serum was also run for comparison. The washes contained excess unbound proteins.

The protein bands present on the corona ranged from 25 kDa to about 150 kDa. Qualitative identification of protein bands was performed based on their molecular weight, and it seemed that most of the bands corresponded to various immunoglobulin heavy and light chains. For quantitative identification of corona proteins, the band was excised and sent to Bioproximity, LLC for Liquid Chromatography Mass Spectrometry (LC-MS). Similar procedure as in gel electrophoresis was followed. Gel was run for only 10 minutes to ensure all proteins from the nanoparticle-protein complex ran into the stacking layer of the gel, but do not reach the resolving layer where they actually start to separate. Based on the results sent by Bioproximity, Table 4 summarizes the proteins found in the corona.

Table 4: Identification of corona proteins by LC-MS (n = 1)

Protein Family Name	**Spectral Count**	**MW (kDa)**
Ig mu chain C region	288	49.3-65.7
Ig gamma-1 chain C region	211	36.1-52.4
Lipoprotein B	126	10.2-92.6, 489.8-515.6
Serum albumin	110	22.9, 45.1-69.4
Complement C3	95	11.2-26.1, 187.1
Ig kappa chain C region	69	11.6-25.6
Ig gamma-3 chain C region	68	41.3-57.1
Complement H	67	6.6-7.7, 43.8-51.0

Immunoglobulins were found to be present in a higher percentage than other protein class. Serum albumin, the most abundant protein in serum, was found to be in less amount than immunoglobulin gamma-1 chain C and lipoprotein B based on the mass spectrometry results. The dark band around 50 kDa (Figure 9) represents immunoglobulin chain C. Serum albumin doesn't have a distinct band on the gel even though it was found to be the fourth most abundant protein in the mass spectrometry analysis. This possibly could be related to the smearing of the albumin band between 50-75 kDa region. A faint band seen at around 180 kDa on the gel corresponds to Complement C3 (mw = 187.1 kDa), which was verified in the mass spectrometry results.

A previous study has shown that albumin, fibrinogen, kininogen-1, complement C9, Ig gamma heavy chain, complement C9, apolipoprotein A1 are the major composition in the protein corona of TiO_2 NPs, with primary particle size of 21nm (21). Another study done on 100-120 nm sized TiO_2 NPs showed that the major proteins in the corona were alpha-2-macroglobulin, serotransferrin, and albumin (22). Based

on these results, it could be inferred that the protein corona composition could differ depending on the particle size. Although it can be seen that albumin is present as a corona protein, which is similar to previous studies. The mechanism of TiO_2 NPs uptake could be similar to that of polystyrene nanoparticles shown in previous study (19). TiO_2 NPs could bind to either albumin receptor or scavenger receptors, however, further experiments are needed to explore this mechanism further.

CHAPTER 3

CELLULAR INTERACTION AND TOXICITY

3.1 Nanoparticle uptake in HeLa cells

Human cervical cancer cells (HeLa) cells were cultured in five 35-mm glass bottom cells culture dishes (MatTek) prior to TiO_2 NPs exposure. The cells were grown in a 5% carbon dioxide atmosphere at 37 °C in minimum essential medium (MEM, Invitrogen, 61100061) supplemented with 10% (v/v) fetal bovine serum (FBS, Invitrogen, 10437-028). After the dishes were confluent enough (>95%) the cells were incubated with increasing concentrations of TiO_2 nanoparticles (0 µg/mL – 1240 µg/mL) for 24 hours at 37 °C.

After 24 hours, the cell culture media was aspirated and the dishes were washed twice with phosphate buffered saline (PBS). The cells were imaged with a Brightfield microscope (Olympus 1X71, Center Valley, PA) using a 60X/1.20W, water immersion objective (UPLSAP060XW, Olympus). Images were taken with an EMCCD camera (DU-897, Andor, South Windsor, CT). The exposure time and gain were 300 ms and 5 respectively. All images were analyzed using ImageJ (NIH)

A large number of black spots can be seen in the cells treated with TiO_2 NPs (fig 1), which is not observed in the control cells. These images show that the cells are interacting with the particles, either through binding onto the cell surface or through internalization through the cell membrane.

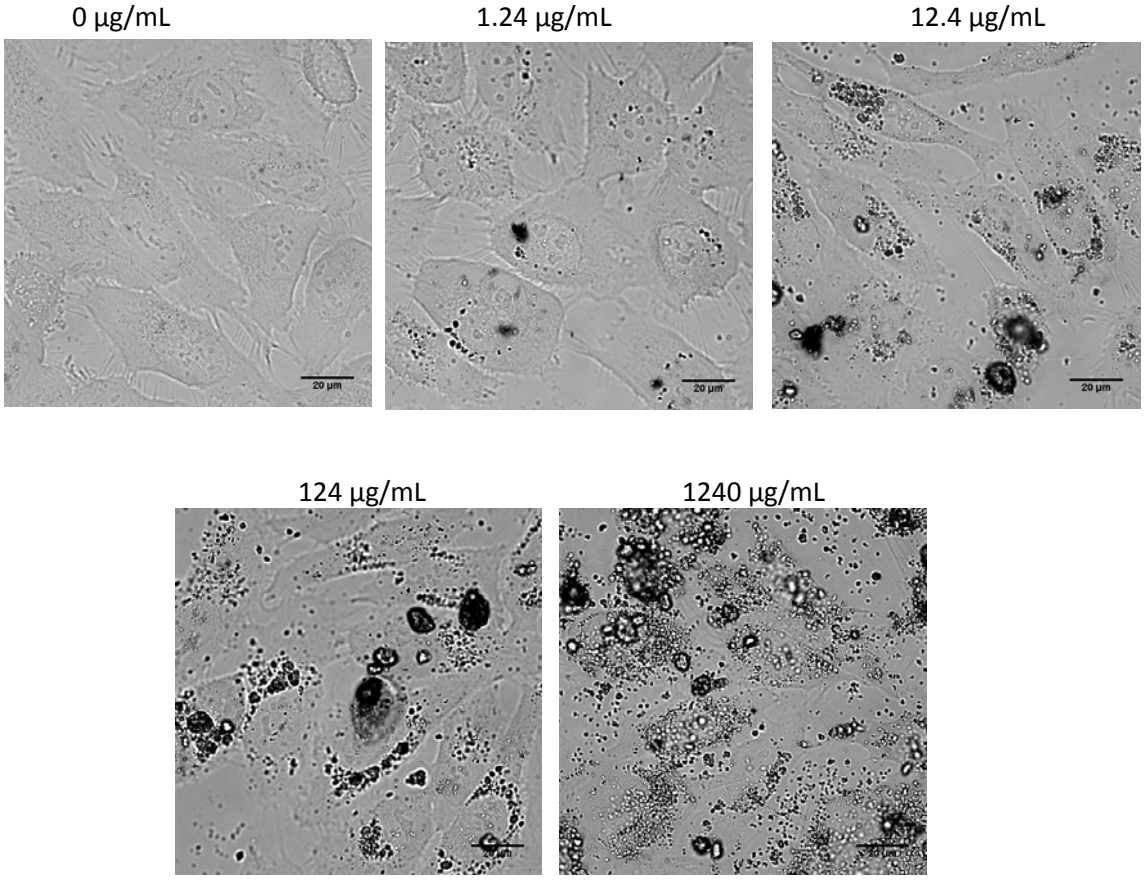

Fig 10: Bright-field microscopy images of HeLa cells exposed to TiO_2 NPs at concentrations shown on top of the images. TiO_2 NPs appear as black spots inside and around the cell membrane.

3.2 MTT assay – cell viability

The Vybrant® MTT cell Proliferation Assay Kit (Life Technologies, V13154) was used to measure cell viability after cells were incubated with TiO_2 nanoparticles for 24 hours. The main purpose of performing this assay is to determine the concentration of TiO_2 NPs which would not affect the cell viability, but still might induce enough oxidative stress to alter the level of gene expression.

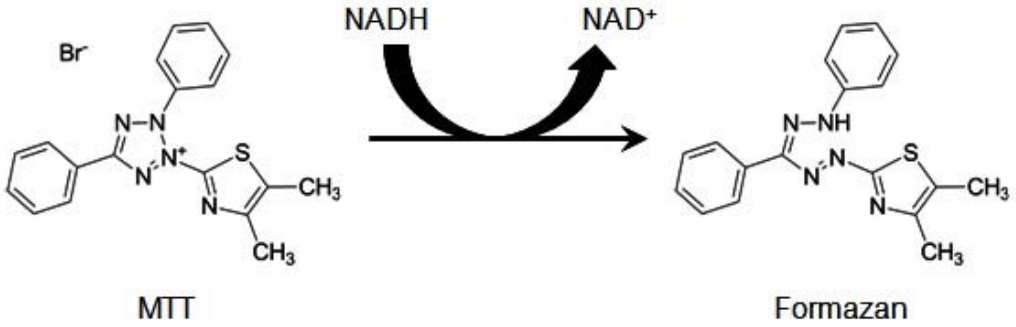

Fig 11: Conversion of tetrazolium MTT compound to formazan involving NADH (23)

The MTT assay utilizes the conversion of water soluble MTT (3-(4,5-dimethylthiazol-2-yl)-2,5-diphenyltetrazolium bromide), which is yellow in color, to an insoluble formazan, which is purple in color. The formazan is then solubilized in dimethyl sulfoxide (DMSO) and an absorbance reading is measured at 540 nm. Only viable cells with active mitochondrial metabolism convert MTT into the formazan product. When cells die, they lose this ability and thus the MTT assay serves as a useful tool in determining number of viable cells.

A MTT stock solution (12mM) was prepared by adding 1 mL of phosphate buffered saline (PBS) to one 5 mg vial of MTT component A. The mixture was vortexed and then sonicated for 10 minutes before storage at 4 °C for 24 hours. The cells were cultured in a 24-well plates (# 15705-060, Falcon) and were incubated with TiO_2 nanoparticles for 24 hours at 37 °C. The concentration of the nanoparticles ranged from 0.124 µg/mL to 1240 µg/mL.

The cell culture medium was aspirated and the wells were replaced with 100 µL of clear MEM after rinsing once. Component A (10 µL) was added to each well for a total volume of 110 µL. The wells were gently swirled to mix and incubated at 37 °C for 4 hours. The mixture (75 µL) was replaced with 75 µL of

DMSO. The well was then incubated at 37 °C for 10 minutes. The solution of each well (10 µL) was then transferred to a 96-well plate, and further diluted by adding 80 µL of DMSO. The absorbance at 540 nm was measured using a SpectraMax M2^e (Molecular Devices) plate reader (Table 1).

Table 5: MTT absorbance values for increasing concentrations of TiO_2 NPs

Well	Control	0.124 µg/ml	1.24 µg/ml	12.4 µg/ml	124 µg/ml	1240 µg/ml
1	0.80	0.53	0.77	0.64	0.681	0.79
2	0.52	0.55	0.57	0.53	0.839	0.95
3	0.66	0.46	0.63	0.55	0.782	0.74
4	0.30	0.51	0.73	0.57	0.90	0.90
Avg	0.57	0.51	0.67	0.57	0.80	0.85
Std dev	0.22	0.04	0.09	0.05	0.09	0.09
P values		0.03	0.11	0.01	0.53	0.07
P values vs control		0.66	0.41	0.97	0.11	0.07

All the p-values against control were above 0.05 and suggest that there was no significant difference in absorbance between the control and any of the concentrations. There were however some differences between 0.124 µg/mL - 1.24 µg/mL; and 12.4 µg/mL and 124 µg/mL. This data suggest that any of the concentrations above can be used for the gene expression experiment. The maximum concentration that can be used is 1240 µg/mL, however, with that high of a concentration, the entire surface of the cell culture dish/flask will be covered with TiO_2 NPs. This will have an effect on the experiments since it will induce mechanical stress to the cells as they will have less area to grow. Having such high concentration will also affect lysis of the cells. Therefore, 124 µg/mL was chosen as the optimum concentration.

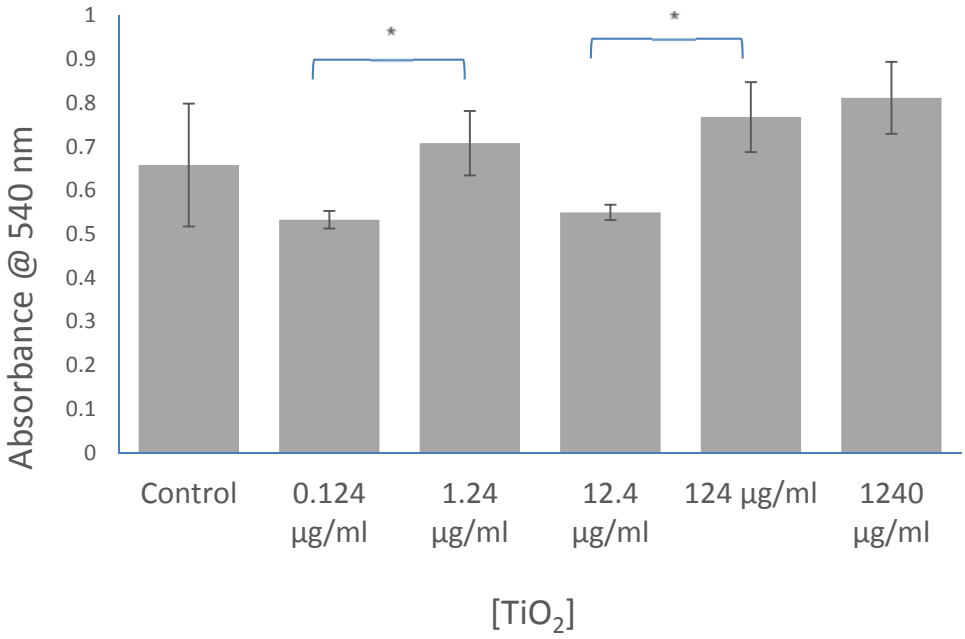

Figure 12: Bar graph of the average absorbance of MTT formazan following incubation of cells with TiO_2 nanoparticles for 24 hours. Error bars represent standard deviation from 3 trials

3.3 LDH assay – membrane permeabilization

Lactase dehydrogenase (LDH) is a cytosolic enzyme present in the cells. There is a release of LDH into the cell culture media if the cell membrane is damaged. Extracellular LDH in the media can be quantified by a coupled enzymatic reaction in which LDH catalyzes a conversion of lactate to pyruvate via NAD+ reduction to NADH. The NADH that is formed is then used to reduce a tetrazolium salt to a red formazan product using diaphorase, which can be measured at 490 nm. Thus, the amount of formazan formation is directly related to the amount of LDH released into the medium, indicative of cytotoxicity.

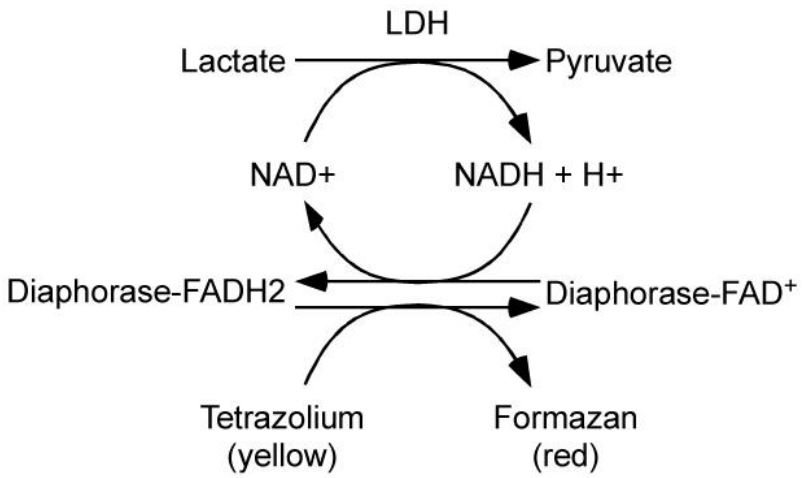

Fig 13. Schematic of LDH assay (24).

HeLa cells were cultured in a 25 cm^2 tissue culture flask (# 353109, Falcon). The cells were trypsinized and number of cells in solution was determined using a hemocytometer. It was calculated that there were 520,000 cells in the solution. Specific volumes of cell solution were added to the 24-well plates (# 15705-060, Falcon). The initial number of cells in the 24 wells were 50000, 75000, 100000 and 75000 (NP treatment) in row1, row2, row3, and row4, respectively. The last row of cells were incubated with TiO_2 nanoparticles, and all the cells were incubated for 24 hours at 37 °C. The medium was aspirated after 24 hours. As controls, sets of triplicate wells were treated only with water (Spontaneous LDH) or with 10X lysis buffer (maximum LDH). The first three rows were used to create a calibration curve of the difference between maximum LDH release and spontaneous LDH release. After treatment with water or lysis buffer, the 24-plate plate was incubated at 37 °C for 45 minutes. Following incubation, 50 µL of solution from each well was transferred to a 96-well plate. To each of the wells in the 96-well plate, 50 µL of the reaction mixture, provided with the kit, was added and incubated at room temperature for in dark for 30 minutes. Stop solution (50 µL), provided with the kit, was added to the wells and absorbance at 490 nm and 680 nm was measured on a microplate reader (SpectraMax $M2^e$, Molecular Devices). LDH activity was determined by subtracting the 680 nm reading (background) from the 490 nm absorbance

values. Percent cytotoxicity was calculated using the equation [(NP LDH activity - spontaneous LDH activity)/ (max LDH activity - spontaneous LDH activity)] × 100%

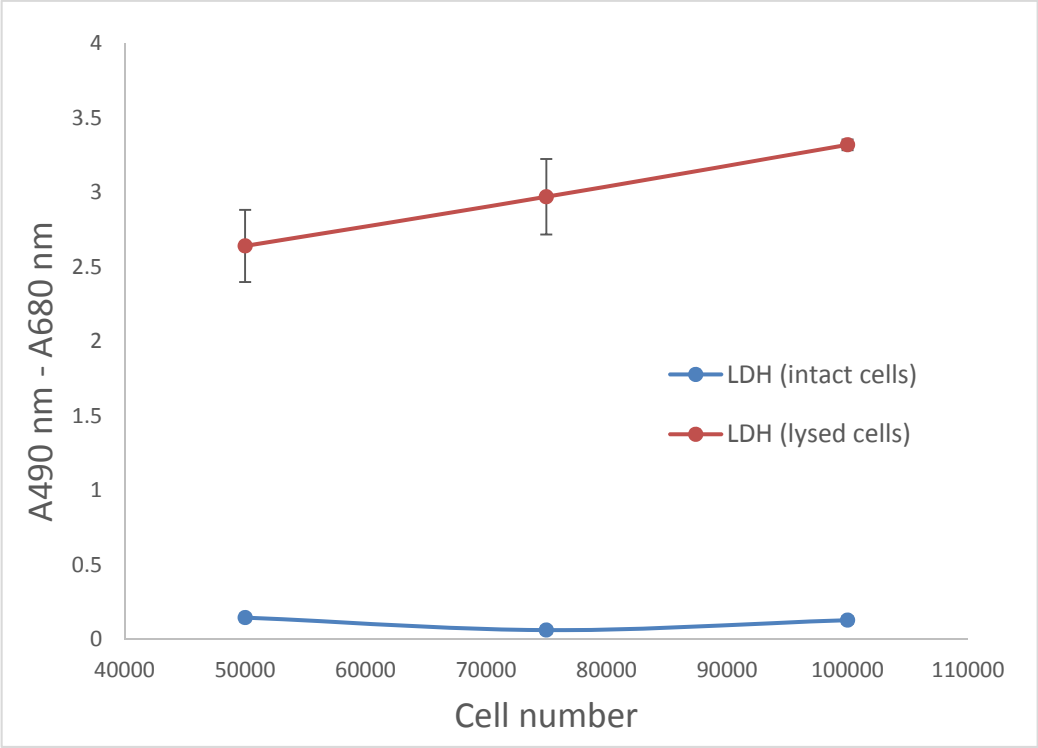

Fig 14. Maximum LDH activity for lysed cells (red) and spontaneous LDH activity for intact cells (blue) are plotted against cell number. The assay was performed in triplicate and error bars represent standard deviation (n = 3). Some error bars are too small to see.

Table 6: Maximum and spontaneous LDH release for control cells and nanoparticle treated cells.

Cell number	**Spontaneous LDH (Abs 490- Abs 680)**			**Spon. Avg**	**Max LDH (Abs 490- Abs 680)**			**Max. Avg**
50000	0.13	0.15	0.16	0.15	2.51	2.98	2.87	2.79
75000	0.09	0.07	0.05	0.06	2.79	3.01	3.30	3.03
100000	0.24	0.08	0.06	0.13	3.43	3.43	3.49	3.45
NP75000	0.09	0.08	0.14		0.09	0.12	0.08	
NP7500 Avg = .10								

As a measure of cell health, LDH assay provides information about the membrane integrity when cells are treated with TiO_2 NPs. Since the nanoparticles we are dealing with are in the form of agglomerates, mechanical disruption of the membrane is possible and LDH will determine if the cells are viable or not. The maximum LDH release does not follow a linear trend (Figure 14), likely due to large number of cells. Further experiments are on-going in the Payne Lab to determine an optimum linear range. An initial percent cytotoxicity of 1.3 % was computed from the absorbance values for nanoparticle treated sample against the control. This percent cytotoxicity is based on cell number of 75000, and further experiments are being carried out to determine cytotoxicity using fewer cells. This preliminary result shows that TiO_2 NPs do not disrupt the cell membrane, although further LDH experiments are necessary.

CHAPTER - 4

OXIDATIVE STRESS INDUCED CHANGES

4.1 Change in gene expression

HeLa cells were incubated with TiO_2 nanoparticles (402 µg/mL, adjusted to concentration per number of cells) in a 25 cm^2 tissue culture flask (# 353109, Falcon) for 24 hours in a 5% carbon dioxide atmosphere at 37 °C. Cells were then lysed and mRNA was extracted using RNeasy® Mini Kit (# 74104, Qiagen) and QIAshredder™ (# 79656, Qiagen). RNA purification was performed using RNase-Free DNase Set (# 79254, Qiagen) to get rid of any genomic DNA contamination. This prevents any genomic DNA from interfering with the subsequent RT-PCR.

The purity and concentration of the isolated RNA was determined using absorbance readings from NanoDrop UV-visible spectrophotometer. The absorbance at 260 nm was used to calculate the concentration, while, the ratio of absorbance at 260 nm and 280 nm was used to assess the purity of the RNA sample. A ratio of 1.8-2.0 indicates that the RNA sample is pure. Table 1 summarizes the RNA concentration and purity for all the trials performed. The ratio is very close to 2 for all three trials, which indicates the extracted RNA was pure. Depending on the concentration of RNA, the volume was adjusted in subsequent experiments to ensure equal amount of RNA was used for cDNA conversion.

Table 7: Summary of RNA concentration and assessment of purity

Trial	**Control**		**TiO_2 Nanoparticle-treated**	
	[RNA] ng/µL	**Abs 260:280**	**[RNA] ng/µL**	**Abs 260:280**
1	1499	2.09	1263	2.08
2	828.7	2.10	1073	2.12
3	892.7	2.10	1026	2.08

Following RNA extraction, copy DNA (cDNA) synthesis was performed using RT^2 First Strand Kit (# 330401, Qiagen). It is crucial for the single stranded RNA to be converted to cDNA before starting the polymerase chain reaction, which makes copies of double stranded DNA. Real-time PCR was performed using RT^2 Profiler™ PCR Array (Human Oxidative Stress Plus, PAHS-065YC-12, # 330231, Qiagen) in combination with RT^2 SYBR® Green ROX™ qPCR Mastermix (# 330522, Qiagen). SteponePlus™ Real-Time PCR System (Applied Biosystems) was used as the real time cycler, in which the first cycle was 10 minutes at 95 °C, and subsequent 40 cycles were at 95 °C for 15 seconds and 60 °C for 1 minute.

Data analysis was performed using GeneGlobe Data Analysis Center (Online, Qiagen) by selecting a baseline threshold cycle (C_T) of 35, and normalizing against housekeeping genes. The five housekeeping genes were beta actin (ACTB), beta-2-macroglobulin (B2M), glyceraldehyde-3-phosphate dehydrogenase (GAPDH), hypoxanthine phosphoribosyltransferase 1 (HPRT1), and large ribosomal protein P0 (RPLP0).

Out of 84 oxidative stress related genes in the PCR array, peroxiredoxin (PRDX) family genes showed change in gene expression. Four out of six PRDX genes showed a significant difference in gene expression across the three trials with a p-value of less than 0.05. PRDX1 and PRDX5 showed an up-regulation whereas PRDX3 and PRDX4 showed a down-regulation against the control. The overall fold regulation for PRDX3 and PRDX4 are 2.7 and 1.8 respectively. Table 2 summarizes the fold change in gene expression of TiO_2 NPs treated cells against the control.

Table 8: Summary of fold change in gene expression

Gene	Fold change	Fold regulation	p-value
PRDX1	1.60	1.60	.014
PRDX3	0.37	2.70	.036
PRDX4	0.56	1.78	.046
PRDX5	1.68	1.68	.011

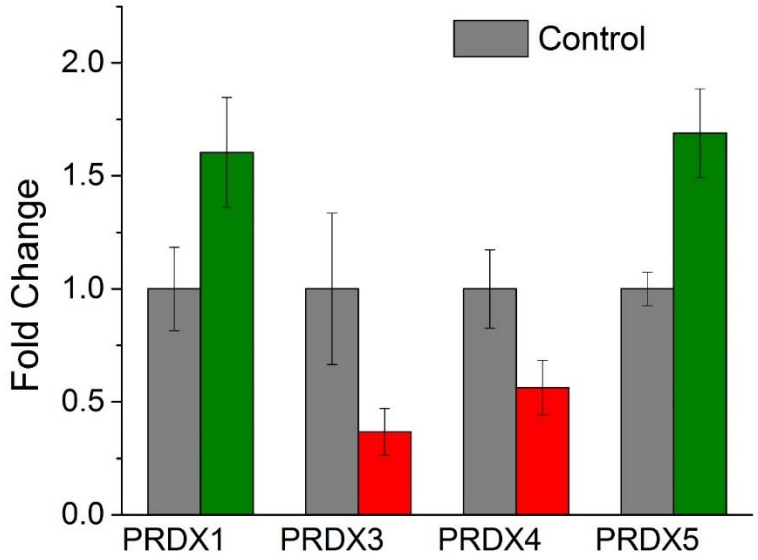

Fig 15: qRT-PCR analysis shows up-regulation (indicated in green) in peroxiredoxin 1 (PRDX1) and peroxiredoxin 5(PRDX5); peroxiredoxin 3 (PRDX3) and peroxiredoxin 4 (PRDX4) are down-regulated (indicated in red). Error bars represent standard error of mean in fold change across three trials.

Based on the gene expression changes, it seems that the peroxiredoxin family genes are the most affected in terms of their expression. There are six mammalian peroxiredoxins and all but PRDX6 have two internal cysteine residues. PRDXs are thiol-specific antioxidant proteins that have a role in protection of cells from ROS-induced cell death. Previous study has shown that these genes are overexpressed in breast cancer cells at the mRNA and protein levels, compared to non-cancerous cells (25). It is also known that PRDX3 is the only protein that localizes in mitochondria out of all the PRDXs (26). However, in our studies, certain PRDXs (PRDX1 and PRDX5) are up-regulated while others (PRDX3 and PRDX4) are down-regulated. This difference in gene expression across the PRDX family needs further investigation.

4.2 Western Blot:

Western Blot is used in cell and molecular biology to identify specific proteins from a mixture of proteins extracted from cells. There are three principle component to this technique: (1) separation of protein by size, (2) transfer to a solid support, and (3) identifying target protein using proper primary and secondary antibodies to visualize (27). Based on the gene expression changes, measured with RT-PCR, peroxiredoxin (PRDX) family genes show a difference in gene expression between cells treated with TiO_2 NPs and control cells. Based on these gene expression changes in the mRNA level we expect a change in the level of protein expression for those genes. Western blot was used to confirm this change in protein expression. PRDX1 and PRDX3 show a change in protein expression at similar levels to that of gene expression change.

Cell lysis:

HeLa cells were incubated with TiO_2 nanoparticles (402 µg/mL, adjusted to concentration per number of cells) in a 25 cm^2 Tissue Culture Flask (# 353109, Falcon) for 24 hours in a 5% carbon dioxide atmosphere at 37 °C. The flask was rinsed with cold phosphate buffered saline (PBS) and trypsin was added to remove the adherent cells. Minimum essential media (MEM) with 10% fetal bovine serum (FBS) was added to inhibit trypsin activity and the suspension was centrifuged at 4000 rpm (4 °C, 5 minutes). The cell pellet was washed with cold PBS and and centrifuged again. The resulting cell pellets were lysed with 100 µL of a lysis buffer containing 1% TritonX-100, 50 mM Tris (pH 8) and 150 mM NaCl. Protease inhibitor (Halt, Pierce 78441) was added with the lysis buffer at a ratio of 1:100. The sample was rocked for 30 minutes at 4 °C, and centrifuged for 20 minutes after. The supernatant, which contains the protein in the absence of cell membrane, was transferred to a new tube and concentration was determined using a bicinchoninic acid (BCA) assay. (Pierce).

Table 9: Concentration of proteins from BCA assay

Trial	**Control cells [Protein] mg/mL**	**NP treated cells [Protein] mg/mL**
1	4.08	2.04
2	2.45	1.73
3	5.68	3.78

Electrophoresis:

Sodium dodecyl sulfate – polyacrylamide gel electrophoresis (SDS-PAGE) was performed on the protein samples in order to separate them based on molecular weight. The protein sample (30 µg) was diluted with 4X Laemmli buffer (1:1) and boiled for 5 minutes at 100 °C. The mixture was loaded into the wells of a precast polyacrylamide gel alongside with 2µL molecular weight marker (928-60000 Chameleon™ Duo Pre-stained Protein Ladder). Tris-glycine SDS running buffer, pH 8.3 (#J61006, Alfa Aesar) was added and the gel was run for one hour at 130 V (50 mA).

Transfer to PVDF membrane:

After electrophoresis was finished the gel was placed in a gel transfer sandwich cassette, which consisted of a PVDF membrane (presoaked in methanol for 2 minutes). The cassette was setup in a transfer apparatus with an ice block and pre-chilled (4 °C) transfer buffer, pH 8.4 (#BP-190, Boston Bioproducts) was added. The transfer was performed at 100 V (275 mA) for an hour.

Antibody incubation:

Blocking buffer (#MB-070, Rockland Immunochemicals) was added to a box containing the PVDF membrane from the transfer step and incubated at 4 °C for an hour with constant agitation. The

membrane was washed with Tris-buffered saline (TBS) for three times, five minutes each. The membrane was incubated with respective primary antibody mixture (table 2) at 4 °C for 18 hours prepared at 1:5000 dilution in blocking buffer. After washing with TBS for 3 times, respective secondary antibody mixture was added to the membrane and incubated at room temperature for an hour. The secondary antibody mixture was prepared at 1:5000 dilution in blocking buffer with the addition of 0.02% SDS. Addition of SDS in small amount helps to eliminate non-specific binding and also reduces background during imaging. IRDye 680LT goat anti-rabbit and IRDye 800CW donkey anti-mouse were the secondary antibodies used. Since, we are using a mixture of primary antibodies, it is important that we use two secondary antibodies that absorb at different wavelengths in the infrared (IR) region. This allows for simultaneous multicolor detection and is essential to compare the target protein band with the housekeeping proteins. The membrane was washed with TBS and imaged using Odyssey Li-cor IR imaging system using software Image Studio Version 3.1.

Table 10: Antibodies and housekeeping proteins

Target protein (molecular weight)	**Housekeeping protein (molecular weight)**	**Primary antibody**	**Secondary antibody**
Peroxiredoxin 1 (PRDX1) 24 kDa	Actin 43 kDa	Rabbit polyclonal to peroxiredoxin 1 (Anti-PRDX1); Mouse monoclonal to actin (Anti-actin)	Goat anti-rabbit 680LT; Donkey anti-mouse 800CW
Peroxiredoxin 3 (PRDX3) 28 kDa	Actin 43 kDa	Rabbit polyclonal to peroxiredoxin 3 (Anti-PRDX3); Mouse monoclonal to actin (Anti-actin)	Goat anti-rabbit 680LT; Donkey anti-mouse 800CW
Sequestosome 1 (SQSTM 1) 48 kDa	GAPDH 37 kDa	Rabbit polyclonal to sequestosome 1 (Anti-SQSTM1); Mouse monoclonal to GAPDH (Anti-GAPDH)	Goat anti-rabbit 680LT; Donkey anti-mouse 800CW

Image analyses:

Densitometry analysis was performed on the membrane images using ImageJ (NIH). Peak area was calculated for the different bands obtained in the gels and the fold change in protein expression was determined by normalizing with the expression of the housekeeping proteins.

Table 11: Overall change in protein expression normalized to housekeeping controls

Target protein	Peak area (Target)		Peak area (Housekeeping)		Housekeeping ratio (NP:Control)	Target protein ratio (NP:Control)	Overall Change
	Control	NP	Control	NP			
PRDX 1	7193	8182	10492	10305	0.98	1.14	1.16
PRDX 1	7307	9662	8164	5073	0.62	1.32	2.13
PRDX 1	3458	3648	8771	8422	0.96	1.06	1.1
PRDX 3	5874	2145	5470	6797	1.24	0.37	3.35

Based on the peak area results, it can be observed that average change in protein expression for peroxiredoxin 1 is 1.46. This overall change is close with the gene expression change of 1.60 for peroxiredoxin 1. Peroxiredoxin 3 also matched with the gene expression change, as it showed around 3.5 fold decrease in protein expression. However, more trials are needed to confirm protein level change in PRDX3. Future experiments will also focus on comparing the level of proteins for genes that have shown a change in regulation.

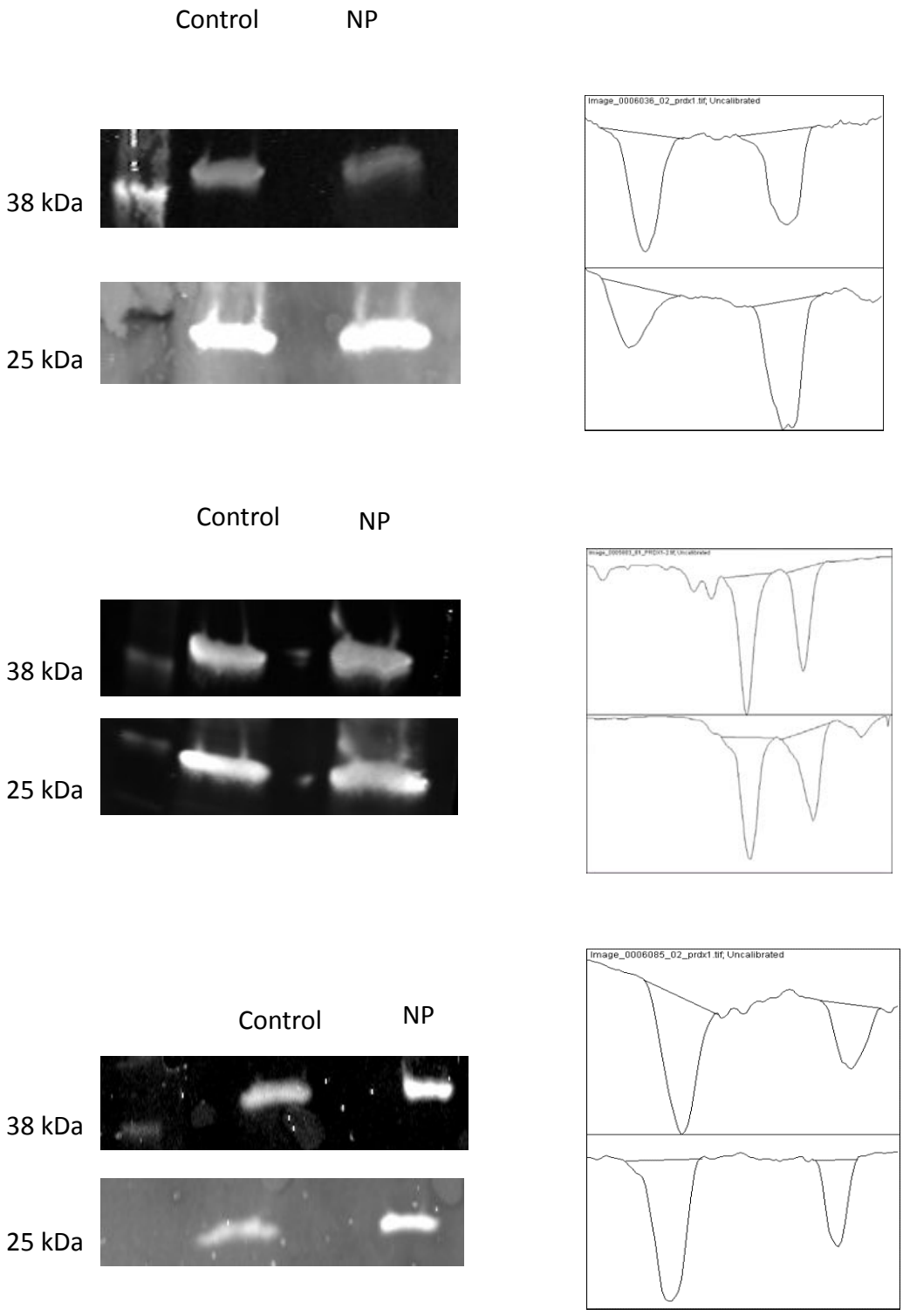

Fig 16: Protein level expression of PRDX1 in cells treated with TiO_2 NPs. Actin (37 kDa) was used as housekeeping gene and PRDX1 (22 kDa) changes were normalized against actin changes. Densitometry analysis is shown on the right.

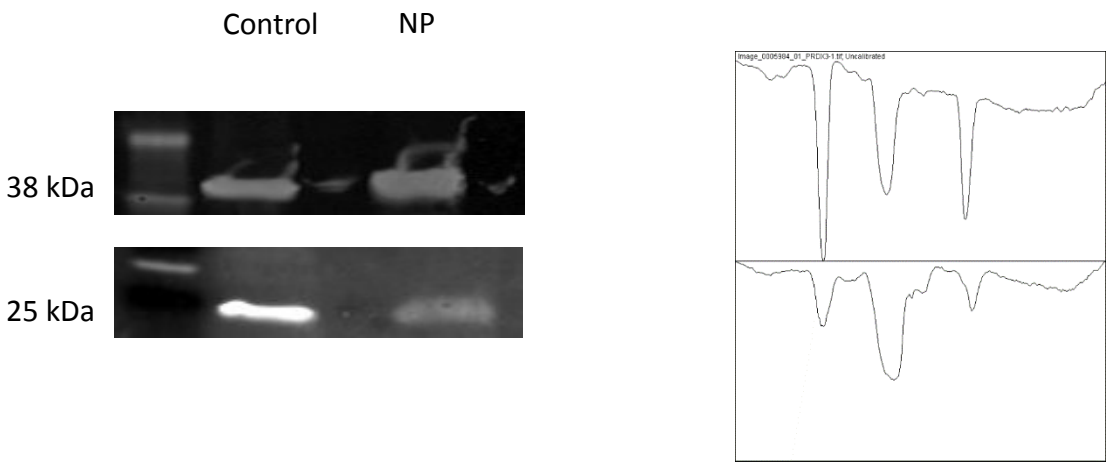

Fig 17: Protein level expression of PRDX3 in cells treated with TiO_2 NPs. Actin (37 kDa) was used as housekeeping gene and PRDX1 (28 kDa) changes were normalized against actin changes

CHAPTER 5

CONCLUSIONS

Overall, we have characterized the size distribution of TiO_2 NPs in water as an environmental model and in the presence of human serum as a biological model. Our data suggests that TiO_2 NPs are in the form of agglomerates rather than individual particles which was verified using TEM and DLS. The median diameter of the agglomerates was found to be 280 nm from TEM images. In the presence of human serum, the median hydrodynamic diameter was 369 nm. Using SDS-PAGE it was verified that the agglomerates have protein corona in the presence of human serum. Based on mass spectrometry data, the protein corona composed of various chains of immunoglobulins, albumin, lipoprotein, and complement proteins. Using brightfield microscopy, it was verified that the cells indeed uptake TiO_2 NPs either by binding or through internalization. Quantitative RT-PCR showed that he nanoparticle protein complex causes a change in gene expression, particularly in the peroxiredoxin (PRDX) family of genes. One possible mechanism of this change in gene expression was attributed to membrane disruption. However, preliminary LDH assay results suggest that TiO_2 NPs do not disrupt the cell membrane, based on a cytotoxicity of 1.3%. MTT assay suggested that the cell health is unaffected with relatively high concentration of TiO_2 NPs (124 ug/ml). The overall mechanism of gene expression is still under investigation. The overall change in mRNA levels for PRDX1 and PRDX3 have been verified by investigating the change in protein levels using western blot. Further experiments are being carried out for the other remaining PRDXs. It could be concluded that TiO_2 NPs in the environment is indeed related with change in gene expression of oxidative stress related genes. Instead of focusing on single pathway, we have looked into an entire range of oxidative stress related genes. This can be further expanded into creating a map of cellular processes that occur after certain genes are regulated. The results from this study could be an important initial finding in investigating toxicity of nanomaterials that are used in daily

life. Even though the focus in this study was on TiO_2 NPs, similar approach could be used to investigate biological and environmental impacts of other nanomaterials.

REFERENCES

1. Kaida, T.; Kobayashi, K.; Adachi, M.; Suzuki, F. Optical characteristics of titanium oxide interference film and the film laminated with oxides and their applications for cosmetics. *J.Cosmetic Sci.,* 2004, *55* (2), 219–220

2. Aitken, R. J.; Chaudhry, M. Q.; Boxall, A. B. A.; Hull, M. Manufacture and use of nanomaterials: current status in the UK and global trends. *Occupat. Med.* 2006, *56*, 300–306

3. Ni M.; Leung M. K. H.; Leung D. Y. C.; Sumathy K. A review and recent developments in photocatalytic water-splitting using TiO_2 for hydrogen production. *Renewable and Sustainable Energy Reviews,* 2007, 11: 401–425

4. Baan R.; Straif K.; Grosse Y.; Secretan B.; El Ghissassi F.; Cogliano V. Carcinogenicity of carbon black, titanium dioxide, and talc. *Lancet Oncol.* 2006, 7: 295–296

5. Landsiedel R.; Ma-Hock L.; Kroll A.; Hahn D.; Schnekenburger J.; Wiench K.; Wohlleben W. Testing Metal-Oxide Nanomaterials for Human Safety. *Advanced Materials*. 2010, 22(24): 2601–2627

6. Robichaud et al, Estimates of Upper Bounds and Trends in Nano-TiO_2 Production As a Basis for Exposure Assessment. *Environ. Sci. Technol*., 2009, 43(12): 4227-4233

7. Shi, H.; Magaye, R.; Castranova, V.; and Zhao, J. Titanium dioxide nanoparticles: a review of current toxicological data, *Particle and Fibre Toxicology,* 2013, 10: 15

8. Senzui M.; Tamura T.; Miura K.; Ikarashi Y.; Watanabe Y.; Fujii M. Study on penetration of titanium dioxide (TiO_2) nanoparticles into intact and damaged skin in vitro. *J Toxicol Sci* 2010, 35: 107–113

9. Wang et al, Acute toxicity and biodistribution of different sized titanium dioxide particles in mice after oral administration, *Toxicol. Lett.* 2007; 168(2): 176-185

10. Andreescu, S. et al, In Oxidative Stress: Diagnostics, Prevention, and Therapy, *ACS Symposium Series; American Chemical Society*: Washington, DC, 2011

11. Boland S.; Hussian S.; and Baeza-Squiban, A. Carbon black and titanium dioxide nanoparticles induce distinct molecular mechanism of toxicity, *Nanomed Nanobiotechnol* 2014, 6:641–652

12. Tay, C.; Cai, P.; Setyawati, M.; Fang, W.; Tan, L.; Hong, C.; Chen, X.; and Leong, D. Nanoparticles Strengthen Intracellular Tension and Retard Cellular Migration, *Nano Letters,* 2014, 14: 83-88,

13. Nel A., Xia, T., Madler, L., Li, N. Toxic Potential of Materials at the Nanolevel, *Science*, 2006, 311: 622-627

14. Xia, T. et al, Comparison of the Abilities of Ambient and Manufactured Nanoparticles to Induce Cellular Toxicity According to an Oxidative Stress Paradigm, *Nano Lett.*, 2006, *6* (8), pp 1794–1807

15. Tedja, R., Marquis, C.; Lim, M.; Amal, R. Biological impacts of TiO_2 on human lung cell lines A549 and H1299: particle size distribution effects, *J Nanopart Res* (2011) 13:3801–3813

16. Long et al, Titanium Dioxide (P25) Produces Reactive Oxygen Species in Immortalized Brain Microglia (BV2): Implications for Nanoparticle Neurotoxicity, *Environ. Sci. Technol.*, 2006, *40* (14): 4346–4352

17. Adkins J.N. et al. Toward a human blood serum proteome: analysis by multidimensional separation coupled with mass spectrometry. *Molecular and Cellular Proteomics*, 2002, 1 (12): 947–955

18. Doorley, G. W.; and Payne, C. K. Cellular binding of nanoparticles in the presence of serum proteins, *Chem. Commun.*, 2011, 47, 466-468

19. Fleischer, C.C.; and Payne, C.K., Nanoparticle surface charge mediates the cellular receptors used by protein-nanoparticle complexes, *J. Phys. Chem. B,* 2012, 116, 8901-8907

20. Kippner, L.E.; Finn, N.A.; Shukla, S.; and Kemp, M.L. Systemic remodeling of the redox regulatory network due to RNAi perturbations of glutaredoxin 1, thioredoxin 1, and glucose-6-phosphate dehydrogenase. *BMC Systems Biology*, 2011, 13(5): 164

21. Deng, G.; Mortimer, G.; Schiller, T.; Musumeci, A.; Martin, D.; and Minchin, R. Differential plasma protein binding to metal oxide nanoparticles, *Nanotechnology,* 20, 455101, 2009

22. Borgognoni, C.F. et al, Reaction of human macrophages on protein corona covered TiO2 nanoparticles. *Nanomedicine NBM,* 2015, 11:275-282

23. Sittampalam, G.S.; Coussens N.P.; Nelson H. et al. *Assay Guidance Manual. Bethesda (MD): Eli Lilly & Company and the National Center for Advancing Translational Sciences*; 2004

24. Decker, T.; and Lohmann-Matthes, M. L.; A quick and simple method for the quantitation of lactate dehydrogenase release in measurements of cellular cytotoxicity and tumor necrosis factor (TNF) activity, *J. Immunol. Methods*, 1988, 115, 61

25. Tehan, L.; Taparra, K.; and Phelan, S.; Peroxiredoxin Overexpression in MCF-7 Breast Cancer Cells and Regulation by Cell Proliferation and Oxidative Stress. *Cancer Investigation*, 31: 374-384, 2013

26. Kayashima, Y.; and Yamakawa-Kobayashi, K. Involvement of Prx3, a *Drosophila* ortholog of the thiol-dependent peroxidase PRDX3, in age-dependent oxidative stress resistance. *Biomedical Research* 33(5): 319-322, 2012

27. Mahmood, T.; and Yang, P.C. (2012). Western Blot: Technique, Theory, and Trouble Shooting. *North American Journal of Medical Sciences*, *4*(9), 429–434